Solvation Effects in the Quartz Crystal Microbalance with Dissipation Monitoring Response to Biomolecular Adsorption. A Phenomenological Approach

ARTICLE *in* ANALYTICAL CHEMISTRY · JANUARY 2009

Impact Factor: 5.64 · DOI: 10.1021/ac8011686 · Source: PubMed

5 AUTHORS, INCLUDING:

Pit Bingen
Collège des Ingénieurs
10 PUBLICATIONS **241** CITATIONS
SEE PROFILE

Nicole F Steinmetz
Case Western Reserve University
79 PUBLICATIONS **1,594** CITATIONS
SEE PROFILE

Ralf P. Richter
CIC biomaGUNE
58 PUBLICATIONS **2,578** CITATIONS
SEE PROFILE

Anal. Chem. **2008,** *80,* 8880–8890

Articles

Solvation Effects in the Quartz Crystal Microbalance with Dissipation Monitoring Response to Biomolecular Adsorption. A Phenomenological Approach

Pit Bingen,[†] Guoliang Wang,[‡] Nicole F. Steinmetz,[§,||] Michael Rodahl,[‡] and Ralf P. Richter*[,†,⊥]

Biosurfaces Unit, CIC biomaGUNE, Paseo Miramon 182, 20009 Donostia, San Sebastian, Spain, Department of Biophysical Chemistry, University of Heidelberg, INF 253, 69120 Heidelberg, Germany, and Department of New Materials and Biosystems, Max-Planck-Institute for Metals Research, Heisenbergstrasse 3, 70569 Stuttgart, Germany, Q-Sense AB, Hängpilsgatan 7, 42677 Västra Frölunda, Sweden, and Department of Biological Chemistry, John Innes Centre, Norwich, NR4 7UH, U.K.

Quartz crystal microbalance with dissipation monitoring (QCM-D) has become a popular tool to investigate biomolecular adsorption phenomena at surfaces. In contrast to optical mass-sensitive techniques, which commonly detect the adsorbed nonhydrated mass, the mechanically coupled mass measured by QCM-D includes a significant amount of water. A mechanistic and quantitative picture of how the surrounding liquid couples to the deposited solutes has so far been elusive for apparently simple phenomena like the random adsorption of nanometer-sized particles on a planar surface. Using a setup that enables simultaneous measurements by reflectometry and QCM-D on the same support, we have quantified the variations in coupled water, as sensed by the QCM frequency response, as a function of coverage for the formation of monolayers of globular proteins, virus particles, and small unilamellar vesicles. We found a close-to-linear relationship between the surface coverage and the relative contribution of water to the frequency response for these adsorption scenarios. The experimental hydration curves could be reproduced quantitatively using a theoretical model that assigns a pyramid-shaped hydration coat to each adsorbed particle and that accounts for the random distribution of adsorbents on the surface. This simple model fits the experimental data well and provides insight into the parameters that affect hydration.

Quartz crystal microbalance with dissipation monitoring (QCM-D) has become a popular tool for the investigation of biomolecular adsorption. The measured responses, resonance frequency, f, and energy dissipation, D, provide time-resolved information about adsorbed masses, and the thickness, morphology, and mechanical properties of interfacial films (cf. refs 1−3 and references therein). Because of its acousto-mechanical transducer principle, the technique is not only sensitive to the adsorbed molecules but also to the solvent into which the interfacial layer is immersed. A number of theories have been developed to reproduce the effects that the solvent imparts on the shear oscillation of the sensor crystal, either as semi-infinite bulk solution or as part of the (viscoelastic) interfacial film.[4−7] These models typically assume the interfacial film to be smooth and homogeneous. In contrast, adsorption processes such as the formation of a protein monolayer on a flat surface, proceed by their very nature via rough and heterogeneous surface morphologies, with the roughness varying throughout the adsorption process. Theoretical treatments that describe the effect of roughness of different scale and nature on the QCM-D response are available (cf. refs 8 and 9 and references therein). It is, for example, established that solvent that is confined in cavities of a rigid support is sensed as if it was a rigid part of the sensor surface.[10] None of these models, however, can

* Corresponding author. E-mail: rrichter@cicbiomagune.es. Phone: +34 943 0053 29. Fax: +34 943 0053 15.

[†] Department of Biophysical Chemistry, University of Heidelberg and Department of New Materials and Biosystems, Max-Planck-Institute for Metals Research.

[‡] Q-Sense AB.

[§] John Innes Centre.

[||] Present Address: Department of Cell Biology, The Scripps Research Institute, La Jolla, CA 92037.

[⊥] Biosurfaces Unit, CIC biomaGUNE.

(1) Höök, F.; Larsson, C.; Fant, C. In *Encyclopedia of Surface and Colloid Science*; Marcel Dekker, Inc.: New York, 2002; pp 774−791.
(2) Hübsch, E.; Ball, V.; Senger, B.; Decher, G.; Voegel, J.-C.; Schaaf, P. *Langmuir* **2004**, *20*, 1980–1985.
(3) Richter, R. P.; Bérat, R.; Brisson, A. R. *Langmuir* **2006**, *22*, 3497–3505.
(4) Kanazawa, K. K.; Gordon, J. G., III *Anal. Chem.* **1985**, *57*, 1770–1771.
(5) Martin, S. J.; Frye, G. C.; Wessendorf, K. O. *Sens. Actuators, A* **1994**, *44*, 209–218.
(6) Domack, A.; Prucker, O.; Rühe, J.; Johannsmann, D. *Phys. Rev. E* **1997**, *56*, 680–689.
(7) Voinova, M. V.; Rodahl, M.; Jonson, M.; Kasemo, B. *Phys. Scr.* **1999**, *59*, 391–396.
(8) Daikhin, L.; Gileadi, E.; Katz, G.; Tsionsky, V.; Urbakh, M.; Zagidulin, D. *Anal. Chem.* **2002**, *74*, 554–561.
(9) Urbakh, M.; Tsionsky, V.; Gileadi, E.; Daikhin, L. In *Piezoelectric Sensors*; Janshoff, A., Steinem, C. Eds.; Springer Verlag: Berlin, Germany, 2006; pp 111−150.
(10) Martin, S. J.; Frye, G. C.; Ricco, A. J.; Senturia, S. D. *Anal. Chem.* **1993**, *65*, 2910–2922.

10.1021/ac8011686 CCC: $40.75
Published on Web 10/01/2008

presently provide direct and quantitative predictions for the effect of water in the specific case of biomolecular adsorption even though this is one of the most common applications of the QCM-D technique. This limits the interpretation of QCM-D responses. In particular, it is difficult to extract the biomolecular mass from the QCM frequency response alone, i.e., to separate the contribution of the adsorbate from the contribution of the solvent that is coupled to it.

Another family of techniques, based on various optical transducer principles, such as surface plasmon resonance, waveguide spectroscopy, ellipsometry, or reflectometry, can provide information on biomolecular mass more directly. These methods are sensitive to differences in the optical density between adsorbate and bulk solution and thus essentially sense the adsorbate mass. The combination of a mass-sensitive optical technique and QCM-D can hence be exploited to characterize the hydration state of soft layers.[6,11−15]

The present study aimed to better understand the role of solvent in the QCM-D response for biomolecular adsorption processes. To this end, we determined the contribution of the solvent to the QCM-D frequency response by using a technical setup that combines reflectometry and QCM-D on the same surface. We present data for the variations in hydration throughout adsorption processes for a number of model systems, including proteins, virus particles, and lipid vesicles. Many of these films have already been characterized in detail and thus represent well-controlled model systems. Motivated by an unexpectedly simple linear relationship between the relative contribution of solvent to the frequency response and the surface coverage, we developed a phenomenological model that can quantitatively reproduce the measured responses. In the framework of this study, we focus on biomolecular films that by themselves induce no or only minor energy dissipation, i.e., for which viscoelastic contributions to the frequency shift are minor.

MATERIALS AND METHODS

Materials. Lyophilized dioleoylphosphatidylcholine (DOPC) and dioleoylphospatidylethanolamine-CAP-biotin (DOPE-CAP-Biotin) were purchased from Avanti Polar Lipids (Alabaster, AL). Lyophilized streptavidin (SAv), lyophilized avidin (Av), and other chemicals were purchased from Sigma. Biotinylated *Cowpea mosaic virus* (CPMV) was prepared as described previously.[16] Ultrapure water with a resistivity of 18.2 MΩ was used. A buffer solution made of 150 mM NaCl, 3 mM NaN_3, and 10 mM HEPES, pH 7.4, was prepared in ultrapure water. $CaCl_2$ (2 mM) was added for all adsorption measurements. EDTA (2 mM) was added instead for the preparation of lipid vesicle stock solutions.

Lipid mixtures containing DOPE-CAP-Biotin and DOPC in a mole mixture of 1:9 were prepared in chloroform, dried, resuspended in buffer solution at 1−5 mg/mL final concentration, homogenized and tip-sonicated, as described earlier,[17] to obtain stock solutions of small unilamellar vesicles (SUVs). Concentrations and mixing ratios were estimated from the dry masses of employed lipid material. Before use, vesicle suspensions were diluted to approximately 50 μg/mL. SAv and Av were reconstituted in ultrapure water to a concentration of approximately 1 mg/mL as described by the manufacturer. Before use, the solutions of SAv, Av, and CPMV were diluted in buffer solution to about 20 μg/mL.

Substrates. Purpose-designed QCM-D sensors with a fundamental resonance frequency of 4.95 ± 0.02 MHz, coated with either silica or gold were provided by Q-Sense (Västra Frölunda, Sweden). Silica-coated sensors were cleaned by immersion in a 2% (w/v) sodium dodecyl sulfate solution for 30 min, rinsing with ultrapure water, and blow-drying with nitrogen. Gold-coated sensors were pretreated by rinsing with ultrapure water and blow-drying with nitrogen. Cleaned substrates were stored in air and exposed to UV/ozone (Bioforce, Ames, IA) for 30 min prior to use.

Combination of QCM-D and Reflectometry. We employed a prototype setup that allows for simultaneous measurements by reflectometry and QCM-D on the same support. Details of the technical implementation are described elsewhere.[18] If not otherwise stated, the system was operated in flow mode, i.e., sample solution was continuously delivered to the measurement chamber (~100 μL volume) by a peristaltic pump (ISM935C, Ismatec, Zürich, Switzerland), using flow rates between 20 and 100 μL/min. In order to switch between sample liquids, the flow was interrupted for a few seconds without disturbing the measured signals. Occasionally, the operation was in intermittent flow mode, i.e., 300 μL of each new sample solution were injected at high speed (1.2 mL/min) while the flow was turned off during the remainder of the adsorption process. The working temperature was 23 °C.

The QCM-D response, the frequencies, f_i, and dissipations, D_i, for the fundamental and several overtones (i = 1, 3,.., 13), and the optical signal, the ratio, S, of the intensities of the p- and s-polarized light after reflection from the sensor surface, were monitored continuously with a time resolution of better than 1 s, while successively exposing different sample solutions to the surface. Undesired effects in the optical response due to the adsorption of material on a prism that was used to guide the light onto the sensor surface were compensated by using a four detector setup, as described elsewhere.[18] The changes in the optical or mechanical properties of the solution, induced by the addition of solutes, did generally not affect the QCM-D or the reflectometric response significantly, as would be expected for the low solute concentrations (≤50 μg/mL) employed.

The adsorbed mass, m_{qcm}, as sensed by QCM-D, was calculated from the measured changes in frequency, f, according to Sauerbrey's equation:[19]

$$m_{qcm} = -C\frac{\Delta f_i}{i} \quad (1)$$

with the overtone number, i, and the mass sensitivity constant,

(11) Höök, F.; Kasemo, B.; Nylander, T.; Fant, C.; Scott, K.; Elwing, H. *Anal. Chem.* **2001**, *73*, 5796–5804.
(12) Höök, F.; Vörös, J.; Rodahl, M.; Kurrat, R.; Böni, P.; Ramsden, J. J.; Textor, M.; Spencer, N. D.; Tengvall, P.; Gold, J.; Kasemo, B. *Colloids Surf. B* **2002**, *24*, 155–170.
(13) Vörös, J. *Biophys. J.* **2004**, *87*, 553–561.
(14) Plunkett, M. A.; Wang, Z.; Rutland, M. W.; Johannsmann, D. *Langmuir* **2003**, *19*, 6837–6844.
(15) Reimhult, E.; Larsson, C.; Kasemo, B.; Höök, F. *Anal. Chem.* **2004**, *76*, 7211–7220.
(16) Steinmetz, N. F.; Bock, E.; Richter, R. P.; Spatz, J. P.; Lomonossoff, G. P.; Evans, D. J. *Biomacromolecules* **2008**, *9*, 456–462.
(17) Richter, R. P.; Mukhopadhyay, A.; Brisson, A. *Biophys. J.* **2003**, *85*, 3035–3047.
(18) Wang, G.; Rodahl, M.; Edvardsson, M.; Svedhem, S.; Ohlsson, G.; Höök, F.; Kasemo, B. *Rev. Sci. Instrum.* **2008**, *79*, 075107.
(19) Sauerbrey, G. *Z. Phys.* **1959**, *155*, 206–222.

$C = 18.06 \pm 0.15$ ng cm^{-2} Hz^{-1}. Data derived from the ninth overtone (~45 MHz) is presented.

The reflectometric response, S, was employed to quantify the amounts of adsorbing proteins and lipids. Assuming the adsorbed film to be homogeneous with a given thickness, d_{optic}, and refractive index, n, the adsorbed mass can be determined according to[20]

$$m_{optic} = \frac{d_{optic}(n - n_{solvent})}{\frac{dn}{dc}} = \frac{1}{A_s \frac{dn}{dc}} \frac{S - S_1}{S_0} = \frac{1}{A_s \frac{dn}{dc}} \frac{\Delta S}{S_0} \quad (2)$$

S_0 and S_1 are the reflectometric responses of a clean surface immersed in buffer and prior to adsorption of a given layer, respectively. Hence, $S_0 = S_1$ for the first adsorbed layer but $S_0 < S_1$ for additional layers.

For a given solute, the refractive index increment, dn/dc, has been demonstrated to be constant for concentrations up to 0.4 g/mL.[21] Our data for supported vesicular layers and for the adsorption of CPMV were well within this range. For protein monolayers though, the concentrations attained slightly higher values (up to 0.6 g/mL). Even in this case, dn/dc does not change by more than 4%, as determined with the more general two-component Lorentz−Lorenz equation.[22] We employed values of $dn/dc = 0.180$ cm^3/g for streptavidin, avidin, and CPMV,[23,24] and 0.169 cm^3/g for lipids.[15,25]

The sensitivity factor, A_s, depends on the optical setup (angle of incidence, wavelength of the polarized probing beam, and properties of the support and the surrounding solvent). For the employed setup, they were calculated to be 0.052 and 0.064 nm^{-1} on silica and gold, respectively, by using the software WVASE after ellipsometric characterization (J. A. Wollam, Lincoln, NE) of clean sensor surfaces. We note that A_s does also depend on the thickness and the refractive index of the adsorbing film, albeit weakly. Variations in A_s were estimated to be within ±5% for films exhibiting a refractive index of $n - n_{solvent} < 0.2$ and a thickness of <25 nm and ~30 nm, on silica and on gold, respectively. The properties of the films investigated here lie within these ranges.

The hydration as a function of time was calculated as:

$$H = 1 - \frac{m_{optic}}{m_{qcm}} \quad (3)$$

We generally found the hydration values to be reproducible, and independent of flow rate and operation mode, for $m_{optic} > 50$ ng/cm^2. For small adsorbed amounts, noise and minor variations in the liquid distribution in the measurement chamber did though significantly affect the hydration, leading to higher noise and variations between measurements.

Random Sequential Adsorption (RSA) Modeling. Random sequential adsorption of hard spheres was simulated, following a Monte Carlo algorithm described by Adamczyk et al.[26] that we implemented in the software MatLab. Simulations were performed using a grid of 200 × 200 squares of edge length r_{ads} with periodic boundary conditions. Snapshots of the surface arrangement of adsorbed spheres at different coverages, illustrating the random distributions that are typical for RSA, are provided in Figure S-5 in the Supporting Information. At long simulation times, we found the fractional coverage (= coverage in terms of projected surface area) to plateau. After 10^7 Monte Carlo steps (= adsorption attempts), a value of 0.538 was reached. This is close to the jamming limit (= 0.546) that has been established as the maximum RSA coverage[26] and validates the proper function of the algorithm. For the simulation of hydration curves (see below), simulations were typically performed until a fractional coverage corresponding to 90% of the jamming limit was reached.

RESULTS

Hydration in Films of Globular Proteins and Particles. In order to assess the effects of hydration on the QCM-D response, we investigated the adsorption of a selection of globular proteins and protein complexes on planar surfaces: streptavidin (SAv) and avidin (Av) on supported lipid bilayers (SLBs) and CPMV particles on planar gold surfaces. The choice of these model systems was motivated by the desire for robustness and simplicity. First, monolayers of globular proteins commonly generate only minor changes in dissipation,[12,27,28] i.e., viscoelastic effects can be neglected and the frequency changes measured by QCM-D readily transferred into masses using eq 1 (Material and Methods section). Second, the molecules of choice are expected to be stable, i.e., they should not undergo conformational changes upon adsorption. Third, the geometry with which the molecules interact with the surface is well-defined and independent of surface coverage: CPMV particles have an icosahedral symmetry with a spherically averaged diameter of ~28 nm diameter;[29] SAv and Av are well-approximated by a cuboid with edge lengths between 4 and 6 nm; due to their specific interaction with the biotinylated SLB, they are oriented with one of their larger faces toward the membrane.[30,31]

In addition, we investigated the adsorption of small unilamellar vesicles (SUVs) on a streptavidin monolayer. This model system is distinct in that the adsorbing species (vesicles) can undergo shape changes, i.e., flattening, and thus exhibit a considerably smaller aspect ratio[32] than the above-described probes. In order to minimize the effects of viscoelasticity on the QCM-D frequency response, we employed vesicles of the smallest attainable size, i.e., sonicated unilamellar vesicles (SUVs) which typically have an outer diameter of 20−30 nm.[32]

(20) Dijt, J. C.; Cohen Stuart, M. A.; Fleer, G. J. *Adv. Colloid Interface Sci.* **1994**, *50*, 79–101.
(21) De Feijter, J. A.; Benjamins, J.; Veer, F. A. *Biopolymers* **1978**, *17*, 1759–1772.
(22) Corsel, J. W.; Willems, G. M.; Kop, J. M. M.; Cuypers, P. A.; Hermens, W. T. *J. Colloid Interface Sci.* **1986**, *111*, 544–554.
(23) *Handbook of Biochemistry*; CRC Press: Cleveland, OH, 1973.
(24) *Polymer Handbook*, 3rd ed.; Wiley-Interscience: New York, 1989.
(25) Salamon, Z.; Tollin, G. *Biophys. J.* **2001**, *80*, 1557–1567.
(26) Adamczyk, Z.; Zembala, M.; Siwek, B.; Warszynski, P. *J. Colloid Interface Sci.* **1990**, *140*, 123–137.
(27) Höök, F.; Rodahl, M.; Brzezinski, P.; Kasemo, B. *Langmuir* **1998**, *14*, 729.
(28) Richter, R. P.; Brisson, A. *Langmuir* **2004**, *20*, 4609–4613.
(29) Lin, T.; Chen, Z.; Usha, R.; Stauffacher, C. V.; Dai, J. B.; Schmidt, T.; Johnson, J. E. *Virology* **1999**, *265*, 20–34.
(30) Reviakine, I.; Bergsma-Schutter, W.; Brisson, A. *J. Struct. Biol.* **1998**, *121*, 356–361.
(31) Brisson, A.; Bergsma-Schutter, A.; Oling, F.; Lambert, O.; Reviakine, I. *J. Cryst. Growth* **1999**, *196*, 456–470.
(32) Richter, R. P.; Brisson, A. *Biophys. J.* **2005**, *88*, 3422–3433.

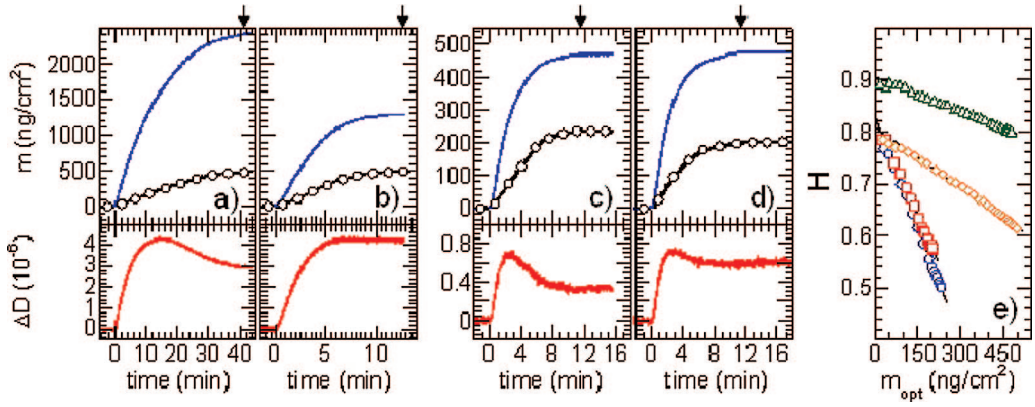

Figure 1. Masses derived from reflectometric responses (m_{opt}, black line with ○, top) and QCM-D responses (m_{qcm}, blue line, top), and QCM-D dissipation shifts (ΔD, red line, bottom) for the adsorption of (a) CPMV particles on gold, (b) biotinylated small umilamellar vesicles (b-SUVs) on a streptavidin (SAv)-covered biotinylated supported lipid bilayer (b-SLB), (c) SAv on a b-SLB, and (d) avidin (Av) on a b-SLB. Exposure of the solutes to the surface started at ~0 min. Times for rinsing with buffer are indicated (arrows). (e) Hydration as a function of optical mass for the measurements shown in parts a–d: CPMV, green △; SAv, blue ○; Av, red □; b-SUVs, orange ◇. The hydration behavior can be fitted well by straight lines (black solid lines) for all four adsorbents (cf. Table 1 for fitting parameters).

Table 1. Total Adsorbed Amounts, As Measured by Reflectometry and by QCM-D, and Parameters Used for Fitting a Straight Line to the Experimental Hydration Curves[a]

	adsorbed amounts		line fit	
sample	m_{optic} (ng/cm²)	m_{qcm} (ng/cm²)	H_0 (10^{-2})	dH/dm_{optic} (10^{-3}cm²/ng)
CPMV	480 ± 20	2440 ± 30	91 ± 1	−0.22 ± 0.02
SAv	240 ± 10	472 ± 10	83 ± 1	−1.41 ± 0.05
Av	205 ± 10	475 ± 10	83 ± 1	−1.24 ± 0.05
SUVs	500 ± 15	1280 ± 10	81 ± 1	−0.38 ± 0.02

[a] Errors correspond to the spread of experimental data, obtained from two to seven measurements per sample (see Figure 1 for representative measurements).

Typical data for the four different adsorption scenarios, given in Figure 1a–d, are consistent with results reported earlier for similar systems, i.e., SAv on biotinylated SLBs,[15,33] CPMV on biotinylated SLBs,[16] and SUVs on gold.[34] In all cases, the adsorbed masses increased monotonously over time. The adsorption rates, as deduced from m_{optic}, were initially constant at magnitudes that match expectations for mass-transport limited adsorption.[35] With increasing coverage, the adsorption rates decreased. The masses deposited by the end of the adsorption process (Table 1) were close to expectations for a dense monolayer in the case of Av and SAv.[15,31] The final adsorbed masses and the dissipation shifts for SUVs are also in accordance with expectations for a densely packed supported vesicular layer.[34] A comparison of the adsorbed mass, m_{optic}, with the molecular weight and dimensions of CPMV particles (Table 2) provides an estimate for the surface coverage of 0.33. No changes in the measured signals were detectable upon rinsing with buffer after the adsorption steps, demonstrating that binding was irreversible. Our data thus confirms the expected formation of fairly dense and stable monolayers in all adsorption scenarios.

The variations in normalized frequency shifts between $i = 3$ and $i = 13$ were smaller than the detection limit for SAv and Av and smaller than 3% of the total response for CPMV (data not shown), confirming that these films do indeed obey eq 1. The frequency shift varied by about 10% for SUVs, indicating that viscoelastic contributions to the frequency shift are not negligible yet still small.

All samples showed small but measurable dissipation signals upon adsorption. Notably, a peak in dissipation at intermediate coverage could be observed for the adsorption of SAv, Av, and CPMV. The subsequent decrease in D indicates an apparent mechanical stabilization of the adsorbed layer with increasing coverage. The exact nature and range of the interactions that give rise to this stabilization are currently not clear and deserve further investigation.

At any given time throughout the adsorption processes, the masses measured by QCM-D were higher than the masses measured by reflectometry and we define the relative difference between both values as hydration (eq 3). It is understood, and will be discussed in detail later on, that this definition is specific to solvation as it is sensed by QCM. It is rather abstract in the sense that we do not make any a priori assumptions about the physicochemical nature of the coupled water. In particular, the definition goes beyond that usually employed to describe the water layer of a few angstroms in thickness that is thought to be tightly associated to molecules or surfaces in an aqueous environment.[36]

Hydration curves, i.e., plots of hydration against optical mass, provide direct insight into the evolution of hydration as a function of coverage (Figure 1e). The hydration decreased with increasing surface coverage. The hydration curves for SAv, Av, and CPMV could be well fitted by a straight line over the entire adsorption range. We find the hydration at high coverage to be compatible with the data by Reimhult et al. For lower coverage, however, our hydration values are significantly (by up to 0.05) smaller. We suggest that the differences are due to the methodological approaches that were employed to convert the QCM-D response into sensed masses. Reimhult et al. used a viscoelastic model (Voinova et al. *Phys. Scr.*

(33) Larsson, C.; Rodahl, M.; Höök, F. *Anal. Chem.* **2003**, *75*, 5080–5087.
(34) Keller, C. A.; Kasemo, B. *Biophys. J.* **1998**, *75*, 1397–1402.
(35) Hermens, W. T.; Benes, M.; Richter, R. P.; Speijer, H. *Biotechnol. Appl. Biochem.* **2004**, *39*, 277–284.
(36) Israelachvili, J.; Wennerström, H. *Nature* **1996**, *379*, 219–225.
(37) Hydration data for the adsorption of SAv on biotinylated SLBs have previously been reported, albeit with a different technical setup: Reimhult, E.; Larsson, C.; Kasemo, B.; Hook, F. *Anal. Chem.* **2004**, *76*, 7211–7220.

Table 2. Parameters Used for Fitting the Truncated Pyramid Model with Random Adsorbent Distribution to the Experimental Hydration Curves[a]

sample	M_w (kDa)	ρ_P (g/cm^3)	$2r$ (nm)	Z	z (nm)	k_A	k_s	H^{int}
CPMV	5400[b]	1.40[b]	28.0 (28[b])	1.86	26.0(28[b])	9.0	1.1	0.61
SAv	60[c]	1.35[e]	5.4 (4.3×5.4[g])	1.52	4.1(4.1[g])	8.0	1.2	0.31
Av	66[c]	1.35[e]	6.0 (5.0×5.6[h])	1.47	4.4(4.0[h])	6.0	1.0	0.41
SUV	3400[d]	1.01[f]	30.0[i]	0.85	12.8	3.8	1.1	0.51

[a] True molecular dimensions are denoted in brackets for comparison. [b] From ref 29, assuming a mixing ratio of 2:9:9 of CPMV-types T, M, and B. [c] Information from the provider. [d] Estimate for SUVs with 25 nm diameter, assuming a membrane thickness of 4 nm and a density of 1.01 g/cm^3. [e] From ref 48. [f] From ref 49. [g] From ref 50. [h] From ref 51. [i] Estimate for SUVs with 25 nm diameter that flatten upon adsorption (cf. ref 32).

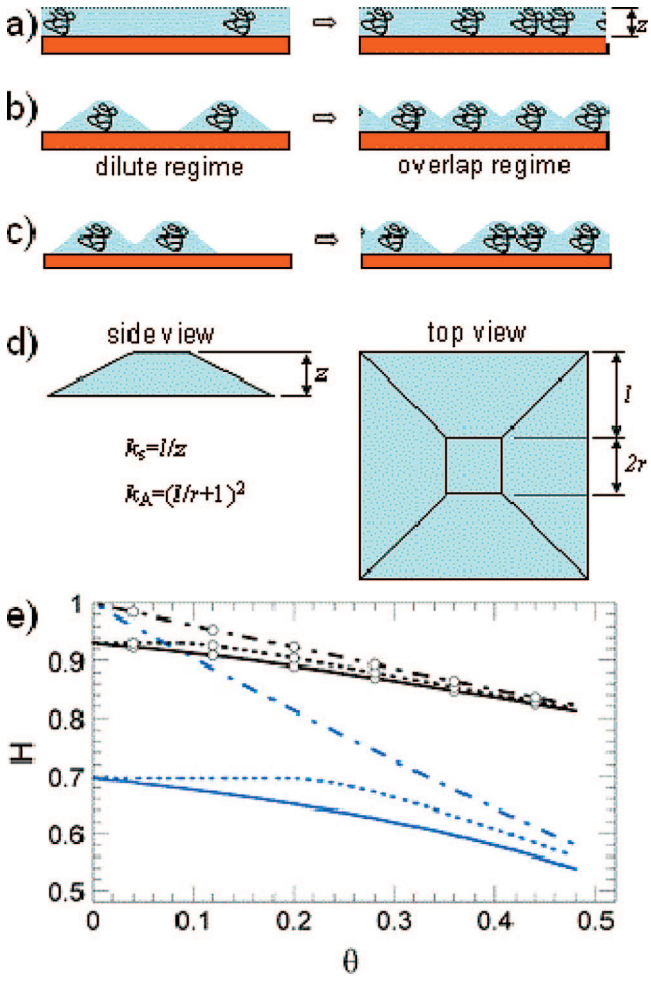

Figure 2. Hydration models. (a) Film of constant thickness (model 1). (b) Truncated pyramid model with regular spacing of adsorbents across the surface (model 2); neighboring hydration pyramids do not overlap at low coverage (diluted regime) but they do at high coverage (overlap regime). (c) Truncated pyramid model with random adsorbent distribution (model 3). (d) Scheme of the truncated pyramid and its dimensions. (e) Predictions of these models (model 1, dashed−dotted lines; model 2, dashed lines; model 3, solid lines) for two different sets of parameters: (i) $r = 3$ nm, $Z = 1$, $k_A = 4$, $M_w = 50$ kDa, and $\rho_P = 1.35$ g/cm^3 (blue lines) and (ii) $r = 15$ nm, $Z = 2$, $k_A = 9$, $M_w = 5000$ kDa, and $\rho_P = 1.35$ g/cm^3 (black lines with ○).

1999, *59*, 391−396). This model assumes a homogeneous film, the applicability of which may be rather limited at low coverage. Indeed, when deriving m_{qcm} via the viscoelastic model, instead of eq 1, we obtained hydration values that agree well with those reported by Reimhult et al.) The linear fit was also reasonable for SUVs, although a slight negative curvature was noticeable. The slopes, dH/dm_{optic}, and hydrations extrapolated to the limit of zero coverage, H_0, were very reproducible (Table 1). CPMV was generally most hydrated and showed the weakest dependence of hydration on coverage. SAv and Av behaved very similar to each other, with minor albeit significant differences in the slope. The hydration of SUVs was similar to SAv and Av at low coverage but showed a weaker dependence on coverage. When $i = 3$ was used instead of $i = 9$, the hydration curve for SUVs remained close-to-linear (data not shown) with a similar slope and a slightly increased $H_0 = 0.83$.

Phenomenological Models of Hydration. The finding of a simple linear relationship between hydration and surface coverage for a range of adsorption scenarios was unexpected and intriguing. What may be the origin of such a response? We sought to reproduce the hydration with a few theoretical models. While varying in complexity, they are all based on the assumption that each molecule carries along a "coat" of water when being adsorbed on the oscillating QCM-D sensor surface. This water coat is treated as a coupled mass that is dragged along with the molecule as the surface oscillates.

This assumption is inspired by two well-known physicochemical phenomena. First, because of the attractive interactions of water molecules with proteins, ions, or surfaces, a water layer of a few angstroms in thickness is usually associated with the solutes.[36] Second, water that is trapped in cavities follows the shear movement of the QCM-D sensor as if it was a rigid body,[5,10] as opposed to bulk water which behaves like a viscous fluid.[4,5] The interior of hollow objects, such as CPMV or SUVs, represent such cavities. Here, we assume in addition that the water that is trapped in the corrugations that are created by particles that adsorb onto a flat and empty surface give rise to a similar response.[10,39] Modeling the full hydrodynamics of the solvent flow in an array of obstacles is computationally intensive and theoretically cumbersome and goes beyond the scope of this work. Here, we model these corrugations by hydration coats of a certain shape. The solvent inside these coats contributes to the frequency shift upon adsorption. All remaining solvent is treated as bulk and as such does not contribute to the frequency shift.

Model 1: Film of Constant Thickness. Starting with the simplest model, we considered a film of constant thickness, z, that becomes populated with solutes throughout the adsorption process (Figure 2a). As the coverage increases, water in the film is gradually replaced by adsorbent. According to this model, the QCM-D senses the entire film as an additional mass as soon as the first particle is deposited on the surface. The thickness of the

(38) Systematic errors on dH/dm_{optic} due to coverage-dependent variations in dn/dc and due to a residual dependence of A_s on the refractive index are estimated to be smaller than 2%. Experimental scatter is given in Table 1.

(39) Dohara, N. *J. Phys. Soc. Jpn.* **1982**, *51*, 4095–4103.

film would correspond to the particle's height. We define the fractional coverage as

$$\theta = \frac{\pi r^2 m}{M_w} \tag{4}$$

m is the adsorbed mass, which corresponds to m_{optic} in our experiment, and M_w the molecular weight of the adsorbent. r is the radius of the adsorbent's footprint (or of the circle that is equivalent to the area of the footprint). The dependence of hydration on coverage can easily be calculated:

$$H = \frac{\pi r^2 z - M_w \rho_P^{-1} \theta}{\pi r^2 z + M_w \left(\rho_{H_2O}^{-1} - \rho_P^{-1}\right)\theta} \tag{5}$$

with $\rho_{H_2}0$ and ρ_P being the densities of buffer and solute, respectively.

For typical values of protein density, adsorbed masses, and layer thickness, we find that the relationship between hydration and coverage is indeed close to linear (Figure 2e), in agreement with our experimental observation. In the context of this model, the hydration in the limit of zero coverage, H_0, would though be unity, in disagreement with our experimental data. This reflects the clearly unrealistic assumption that a single molecule would be sufficient for the QCM-D to sense all water within the film of thickness z as a rigid mass.

Model 2: Pyramid Model (Analytical Solution). To overcome this limitation, we next assumed that the space taken up by an adsorbent and the solvent coupled to it can be approximated by a truncated pyramid as pictured in Figure 2d. The height, z, and the width, $2r$, of the quadratic footprint of the flat central part are thought to represent the dimensions of the adsorbed particle. The extension of the pyramid's quadratic base is described by l. The shape of the truncated pyramid can be conveniently described by form factors: $k_s = l/z$ is a measure for the inclination of the pyramid's sidewalls and hence for its steepness; $k_A = (l/r + 1)^2$ is the relative size of the pyramid base with respect to the footprint of the flat central part. For given r and z, the shape of the pyramid is fully determined by one of these two form factors. The hydration coats are assumed to be aligned with respect to the sensor crystal's oscillatory shear motion, with one of the edges of the pyramid's base being oriented parallel to the direction of motion.

At low coverage ("dilute regime"), the coats that surround adjacent adsorbent particles do not overlap and the hydration is constant. At high coverage ("overlap regime") the pyramids overlap and thereby diminish the average hydration per adsorbed particle (Figure 2b). From the average volume, v, of the hydration coat around each adsorbed particle, the hydration is determined by

$$H = \frac{v - M_w \rho_P^{-1}}{v + M_w \left(\rho_{H_2O}^{-1} - \rho_P^{-1}\right)} \tag{6a}$$

The dependence of v on coverage can be expressed analytically (cf. Supporting Information), if we make the simplifying assumption that the adsorbed particles are arranged in a regular, say, rectangular lattice, at any given coverage. It is convenient to rescale all length scales by r, i.e., $Z = z/r$, $L = l/r$. The reduced volume, $V = v/r^3$, is then

$$V = \frac{4Z}{3}(k_A + \sqrt{k_A} + 1) \tag{6b}$$

for the dilute regime and

$$V = \frac{Z}{3(\sqrt{k_A} - 1)}(3\pi\sqrt{k_A}\theta^{-1} - \pi^{32}\theta^{-32} - 4) \tag{6c}$$

for the overlap regime. The critical coverage, $\theta_c = \pi/(4k_A)$, defines the boundary between the two regimes. From eqs 6a−6c, it can be easily verified that, apart from the parameters that describe the adsorbing particle (r, Z, M_w, and ρ_P), the hydration curve depends solely on the form factor k_A.

At low coverage, the pyramid model predicts hydration values smaller than unity that vary as a function of the adsorbent properties. In the overlap regime, a linear dependence of the hydration on coverage is observed (Figure 2e). The model thus nicely reproduces two essential features of the experimental data. The sharp transition between the dilute regime and the overlap regime around θ_c, however, was not observed experimentally. This can be rationalized by considering the influence of the distribution of adsorbents across the surface: the model assumes a regular arrangement, but in reality, solutes will adsorb at random surface sites and can, at least in the case of adsorption to SLBs, diffuse randomly along the surface. This leads to statistical variations in the distance between an adsorbent particle and its nearest neighbors and hence also in the degree of overlap of neighboring pyramids. This statistical distribution will effectively lower hydration.

Model 3: Pyramid Model with Random Adsorbent Distribution. In order to account for the statistical distribution of adsorbed molecules, we simulated the adsorption of solutes by a popular Monte Carlo algorithm: random sequential adsorption (RSA). The RSA approach has been successfully employed to describe various adsorption processes.[40] The geometry of the projection of the adsorbing particles on the surface was approximated in the simplest way: by hard spheres of radius r_{ads}. Despite its simplicity, the hard sphere approximation is of rather general validity, since even the case of particles exhibiting long-range interactions can often be well described by a hard sphere model if r_{ads} is appropriately chosen.[38] Given the high ionic strength employed in our measurements, the interaction between individual solute molecules is expected to be short-ranged. We therefore chose r_{ads} to be close to the physical dimensions of our solutes ($r_{ads} = r$). The algorithm used in our study differs from those reported previously in that the hydration was calculated after each adsorption step by accounting for the overlap of all hydration coats present on the surface. The relationship between hydration and coverage was thus directly computed.

A few general observations can be made when comparing the analytical solution and the RSA-based solution of the pyramid model for some representative sets of parameter values (Figure 2e). First, in the limits of very low and very high coverage, both models predict similar hydration values. This is not unexpected.

(40) Adamczyk, Z.; Siwek, B.; Zembala, M.; Belouschek, P. *Adv. Colloid Interface Sci.* **1994**, *48*, 151–280.

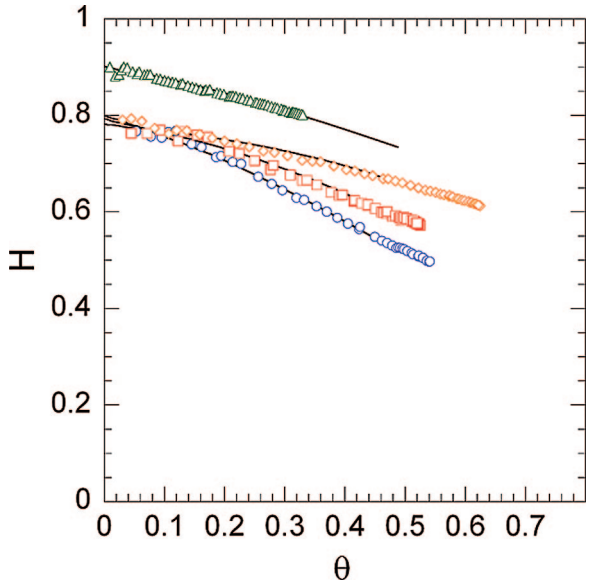

Figure 3. Best fits (black solid lines) to the experimental hydration curves for CPMV (green △), SAv (blue ○), Av (red □) and b-SUVs (orange ◇) (cf. Figure 1), as a function of fractional coverage, using the truncated pyramid model with random adsorbent distribution (model 3). The model can reproduce the hydration of all four adsorbents (cf. Table 2 for fitting parameters) well.

At sufficiently low coverage, the hydration coats of the few adsorbent particles will not overlap and the hydration is therefore given by eqs 6a and 6b, no matter which model is used. Toward maximum coverage, the nearest neighbor distances will be rather small for all adsorbed solutes and the effect of random distribution on hydration becomes small. The good correlation between models 2 and 3 in the limits of low and high coverage thus provides indirect confirmation that the algorithm for computing the hydration within the RSA model worked properly. Second, the deviation between both models is largest around θ_c: when accounting for the random distribution of adsorbent molecules, the sharp transition between the dilute regime and the overlap regime disappears. A fairly (although not entirely) linear relationship between hydration and coverage can now be found over the entire adsorption range, in qualitative agreement with our experimental data.

How well can the model reproduce our data quantitatively? We created a series of hydration curves, generated by Monte Carlo simulation, in order to fit the experimental data for the adsorption of SAv, Av, CPMV, and SUVs. Z and k_A were used as fitting parameters. r, M_w, and ρ_P were fixed at values that are characteristic for each adsorbent (Table 2). The results, shown in Figure 3, provide evidence for an excellent agreement between experimental and theoretical curves for all adsorbent types. The resulting values of z were close to the expected height of the adsorbents (Table 2).

It is instructive to consider the output values of the fitting and their significance in detail. The adsorbent heights, z, were generally well-determined. Changes of only a few angstroms in z induced deviations from the experimental data that could not be balanced by shifts in k_A. The fitted values of z for SAv and Av are in reasonable agreement with the expected height of these molecules. For CPMV, a height of around 26 nm was found, a few nanometers less than the particle size (28 nm). The difference is likely due to a misfit between the spherelike particle shape and the flat geometry in the center of the prismoid-shaped hydration coat. The estimate provided by the model is considerably better than the Sauerbrey equation. With the use of eq 1 and a final hydration of 80%, an effective layer thickness of only 23 nm would be calculated when employing the assumption of a homogeneous layer. The latter approach, although commonly used, thus considerably underestimates the true dimensions of CPMV. The model predicts a height of around 13 nm for SUVs which is within the range of values that have previously been measured for surface-bound vesicles of similar size.[32,42] The uncertainty in z is though somewhat higher than for the adsorption of proteins or virus particles, since vesicles typically exhibit a rather large size distribution[43] and thus only a rough estimate of the average vesicular weight and diameter can be made. In addition, the height determined for SUVs should be considered a lower estimate, due to viscoelastic effects that tend to decrease the measured frequency shift and thus the computed hydration. When using $i = 3$ instead of $i = 9$ to compute m_{qcm}, a height of 14 nm was obtained.

The hydration curves where somewhat less sensitive to variations in k_A: we estimate the relative error for this parameter to be in the range of 10%. k_A decreased monotonously with the aspect ratio Z, from a value of 9 for CPMV ($Z = 1.86$) to around 4 for SUVs ($Z = 0.85$), indicating that there is a direct relationship between these two parameters. Indeed, the form factor k_s, which relates Z and k_A, by $k_sZ = {k_A}^{1/2} - 1$, was very similar (around 1.1) for all investigated adsorbents, indicating that the steepness of the pyramid is independent of the adsorbent type.

We have chosen a pyramid-like shape of the hydration coat, which conveniently rendered our calculations rather simple. From a conceptual point of view, however, this choice was arbitrary, and one may wonder inhowfar the choice of the shape affects the outcome of the model. We tested this by generalizing our model to prismoid-shaped coats (Figure S-1 in the Supporting Information) with rectangular footprints. By introduction of a parameter, k_b, that describes the aspect ratio of the footprint, various shapes can be sampled, ranging from a truncated pyramid to an elongated wedge with two vertical sidewalls. We found the hydration curves to be only very weakly affected by changes in k_b (Supporting Information): the hydration curves were invariant to the geometry of the coat's base as long as the area of the base was maintained. This can be understood intuitively, when considering that the volume inside the prismoid (and the change in effective volume upon overlap of neighboring coats) will stay approximately constant, as long as the area of the footprint is maintained constant. Similar results would be expected for, e.g., truncated cones. This finding justifies the choice of a simple truncated pyramid for our calculations a posteriori.

We note, however, that the above-given arguments do only hold for coat geometries for which any cross section through the z-axis would exhibit straight sides. Hydration curves should be

(41) Simple calculations show that a slightly convex top in the center of the truncated pyramid would easily accommodate the height difference while the volume that is thereby added to the hydration coat would be too small to affect the hydration curve appreciably.

(42) Reviakine, I.; Brisson, A. *Langmuir* **2000**, *16*, 1806–1815.
(43) Coldren, B.; van Zanten, R.; Mackel, M. J.; Zasadzinski, J. A.; Jung, H.-T. *Langmuir* **2003**, *19*, 5632–5639.

different for curved sides. A segment of a sphere, for example, chosen such that its volume is equivalent to a truncated pyramid, would have a smaller footprint and the dilute regime would thus extend to higher coverage (for regular adsorbent spacing) or the decrease in hydration at low coverage would be slower (for random adsorbent distribution). The hydration would though decrease more strongly for medium or high coverages. In qualitative terms, a hydration curve with a more convex shape would thus be obtained. In the interest of keeping our model simple, and given that the fits to the data are quite satisfactory, we refrain from quantifying these effects here.

DISCUSSION

We have analyzed the hydration, as perceived by QCM-D, as a function of coverage for the formation of monolayers of adsorbents of varying size and geometry on various surfaces. For relatively simple adsorption scenarios that are likely not to involve coverage-dependent variations in the conformation and orientation of the adsorbed molecules, we consistently found a close-to-linear relationship between hydration and adsorbed masses. The slope of the hydration curve and the hydration, H_0, in the limit of zero coverage, varied with adsorbent type.

The experimental hydration curves could be reproduced well with a theoretical model that assumes a random distribution of adsorbent molecules and in which a hydration coat, here chosen to be shaped as a truncated prism, is ascribed to each adsorbed particle. Hydration decreases with increasing coverage, as these coats successively overlap with each other. With reasonable values for the dimensions of employed adsorbents, the model could quantitatively reproduce our experimental hydration curves.

What is the nature of the hydration that is sensed by QCM? A fraction of the water will be buried in the interior of the adsorbent or tightly associated to it due to attractive molecular interactions. We will henceforward refer to this fraction as internal hydration. Our results indicate furthermore that water can be coupled to adsorbents at distances that laterally exceed their own nonhydrated dimensions considerably, and we term this fraction external hydration. From a fit of the experimental data to the shape of a truncated pyramid, we conclude that the lateral extension of the coat corresponds at least to the height of the adsorbent; for more elongated shapes, the extension would be even larger. For the adsorbents employed here, these distances correspond to a few nanometers at least, a length scale that is larger than what would be expected for physisorbed or hydrogen-bonded water shells alone. Hence, hydrodynamic coupling must play an important role.[44] Given the predominantly hydrodynamic origin of the external hydration sensed by QCM, we expect the solvation behavior to be very similar for other, at least Newtonian liquids. The properties of the surface, in particular its hydrophilicity, should not strongly affect the hydration as long as no-slip conditions prevail.

It appears reasonable, and it is convenient within the framework of our model, to approximate all water contained inside the central cuboid of height z and footprint $2r \times 2r$ as

(44) Macakova, L.; Blomberg, E.; Claesson, P. M. *Langmuir* **2007**, *23*, 12436–12444.

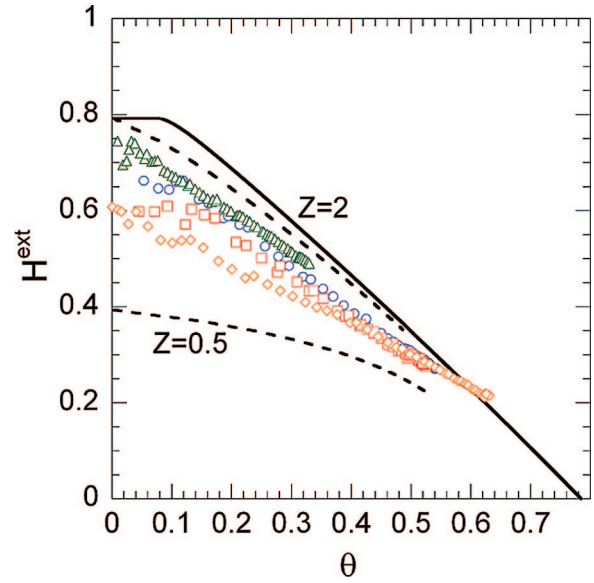

Figure 4. External hydration as a function of coverage, as calculated from eqs 7a and 7b with the parameter values given in Table 2, for the adsorption of CPMV particles on gold (green △), streptavidin (blue ○), and avidin (red □) on a biotinylated SLB, and biotinylated SUVs on a SAv monolayer (orange ◇). The data for CPMV, SAv, and Av fall almost on the same line, indicating that the external hydration is independent of size for particles of similar aspect ratio. For lower aspect ratios, the external hydration decreases, as seen for SUVs. Predictions for $Z = 2$ (solid line, model 2; dashed line, model 3) and $Z = 0.5$ (dashed line, model 3) are also shown, assuming $k_s = 1.1$ and $\rho_P = \rho_{H_2O}$. All data, except for SUVs at highest coverage, lie within the range delimited by these theoretical curves.

internal hydration, while the external hydration makes up the peripheral regions of the prism-shaped coat. The internal hydration, i.e., the relative contribution of water to the mass of the central cuboid,

$$H^{\text{int}} = 1 - \left[1 + \frac{\rho_{H_2O}}{\rho_P}\left(\frac{4r^2 z \rho_P}{M_w} - 1\right)\right]^{-1} \tag{7a}$$

can be considerable and varies strongly for different adsorbents (Table 2). The capsids of CPMV particles, for example, have 60 pores with an opening of about 0.75 nm that allow solvent to diffuse into the internal cavity of the viral particle. This is reflected in the internal hydration which amounts to ~60%. In contrast, the internal hydration for SAv is only ~30%. Such differences affect the hydration curves and contribute appreciably to the variations in the slope and in H_0 that we observed in Figure 3 as a function of adsorbent type.

The relative contribution of the external hydration to the total sensed mass is

$$H^{\text{ext}} = 1 - \frac{1 - H}{1 - H^{\text{int}}} \tag{7b}$$

A comparison of the external hydration for our experimental adsorption scenarios, displayed in Figure 4, reveals several features that differ distinctly from the observations made for the total hydration (Figure 3): (i) the external hydration values for CPMV are only marginally higher than for SAv and Av; (ii) the values for SUVs are considerably lower than those of SAv

and Av at low coverage but they approach these proteins at high coverage. Our analytical model provides a simple rationale to understand these findings. When defining an effective mass, $M_w^{eff} = M_w/(1 - H^{int})$, and an effective density, $\rho_P^{eff} = M_w^{eff}/4r^2z$, for the central cuboid, and when assuming that the difference between ρ_P^{eff} and ρ_{H_2O} is negligible, eqs 6a−6c simplify to

$$H^{ext} = 1 - \frac{12}{3 + 4(k_s Z + 3/2)^2} = 1 - \frac{12}{3 + 4(\sqrt{k_A} + 1/2)^2} \quad (8a)$$

for the dilute regime, and

$$H^{ext} = 1 - \frac{12k_s Z}{3\pi(k_s Z + 1)/\theta - 4 - \pi^{32}/\theta^{32}} = 1 - \frac{12(\sqrt{k_A} - 1)}{3\pi\sqrt{k_A}/\theta - 4 - \pi^{32}/\theta^{32}} \quad (8b)$$

for the overlap regime. The equations highlight that the external hydration does not depend on the size r of the adsorbent, at least if density effects are neglected. Provided that k_s is similar for all adsorbents, as indicated by the fits to our data, it is also directly apparent that it is the adsorbent's aspect ratio Z that determines the external hydration. From eq 8a and $k_s \approx 1.1$ (cf. Table 2), we can estimate the external hydration in the limit of zero coverage to

$$H_0^{ext} \approx 1 - (1 + 1.1Z + 0.4Z^2)^{-1} \quad (8c)$$

These conclusions, here derived with the analytical model, do also hold for random adsorbent distribution. Illustrative theoretical curves for $Z = 2$ and 0.5 are included in Figure 4. As expected, almost all experimental data lie within the area delimited by these two curves. SUVs at high coverage make an exception. The origin of the increased hydration for SUVs at high coverage is currently not clear. SUVs are flexible objects, and we speculate that the height of the adsorbing vesicles may increase slightly with increasing coverage thereby increasing the hydration. We have seen that viscoelastic effects are not entirely negligible for SUVs. Changes in the QCM-D response upon stiffening of the layer at high coverage would lead to an increased apparent hydration and may thus also be responsible for the deviation between model and experiment.

We note in passing that the comparison between model and experiment in Figure 4 should be taken as an approximation. The effective density of the central cuboid exceeds that of water by 22%, 18%, and 13% for SAv, Av, and CPMV, respectively (cf. Table 2). A density increase in this range would lower the theoretical curves in Figure 4 slightly but does not affect the general conclusions outlined above.

A comparison of internal and external hydration provides an explanation for the variations in the total hydration curves in Figure 3. The differences in H between CPMV on one side and SAv or Av on the other side originate predominantly from the differences in the internal hydration of each adsorbent. The similarity in H_0 for SUVs on one hand, and SAv or Av on the other hand, is coincidental, due to a balancing effect of internal hydration (which is higher for SUVs) and external hydration (which is higher for SAv and Av).

The developed hydration model allows for the direct correlation with experimental hydration data. In the following, we will discuss a few consequences of our results and outline potential applications for this methodological approach.

Determining the Height of Adsorbent Particles. The Sauerbrey equation has previously been shown to provide reasonable estimates for the thickness of densely packed monolayers of proteins.[12,13,27,28] We found that this approximation fails for small or intermediate coverage. In the case of CPMV, for example, the estimated thickness of the particle monolayer at 33% coverage, based on the Sauerbrey equation, is 23 nm, i.e., almost 20% less than the particle's dimensions. The same example illustrates that the application of the hydration model to experimental data can provide better estimates of the particle height over the entire coverage range.

Potential Effects of the Organization and Morphology of Adsorbents on Hydration. We have chosen the RSA model to generate a random distribution of molecules on the surface. How accurately does the RSA model represent the experimental adsorption scenarios investigated here? Given the colloidal nature of CPMV[29] and its strong and nonspecific adsorption onto gold surfaces, it is likely that all important assumptions of the model are met, including independent adsorption of individual particles, irreversible adsorption, and absence of lateral mobility of surface-bound particles. AFM images of CPMV on gold (Figure S-4 in the Supporting Information) support this scenario. The RSA approach should thus represent the experimental data well.

For the adsorption of SAv and Av, an important assumption of the RSA model is not met: adsorbed molecules can readily rearrange, and potentially cluster, by diffusion along the SLB. Upon simple lateral diffusion, a random distribution of adsorbent molecules will be maintained, as long as repulsive interparticle interactions are short-ranged and attractive interactions are small. The exact pattern of the random arrangement is likely not to affect the hydration curve strongly, and we do therefore expect the RSA model to be suitable for surface coverages below the jamming limit.

The local accumulation of molecules into clusters or two-dimensional (2D) crystalline islands could though lead to a significant decrease in hydration: the hydration coats of the molecules inside the cluster would overlap much stronger than if the molecules were distributed evenly across the surface. A comparison between models 2 and 3 illustrates that the hydration curve is sensitive to the arrangement of adsorbents on the surface, in particular for low and intermediate coverage. The comparison suggests that a combination of QCM-D and an optical technique may have the discriminative power to distinguish between clusters (which should give lower hydration) and individual molecules. Our methodological approach may thus constitute an interesting and label-free route to investigate clustering events. Likewise, it is conceivable that other morphological features, such as coverage-dependent conformational states of adsorbents, or the presence of two or more adsorbing species, can be detected.

(45) Reviakine, I.; Brisson, A. *Langmuir* **2001**, *17*, 8293–8299.
(46) Richter, R. P.; Brisson, A. *Langmuir* **2003**, *19*, 1632–1640.
(47) Höök, F.; Ray, A.; Nordén, B.; Kasemo, B. *Langmuir* **2001**, *17*, 8305–8312.

To the best of our knowledge, no clustering has yet been reported for Av, but SAv is known for its propensity to form 2D crystals on SLBs. Direct evidence has though only been established for SLBs that were supported by mica[45] or silicon wafers,[46] i.e., surfaces that exhibit a root-mean-square roughness in the angstrom-range. It is to date not clear whether 2D crystallization does also occur on surfaces that exhibit nanometer-scale roughness, such as the sensor surfaces employed here.[46] The pronounced peak in dissipation upon adsorption of SAv (cf. Figure 1b) has previously been proposed as a marker for 2D crystallization[47] but in the light of similar peaks for Av (Figure 1c), CPMV (Figure 1a) and other proteins[48] with low propensity for 2D crystallization, this conclusion appears premature. A comparison between our data for Av and SAv did not reveal any particular difference in the hydration behavior, except for a minor difference in the overall slope of the hydration curve (Figure 1d). Crystallization of SAv was though reported to set in at rather high surface coverage,[49] i.e., in a regime in which the differences in hydration are expected to be small and hence the sensitivity of our technical approach to discriminate between different arrangements on the surface is likely to be rather low. It remains therefore unclear if SAv does crystallize on the SLBs investigated here.

Effects of Hydration on Sensitivity. The dependence of hydration on coverage also directly implies that the sensitivity of the QCM for an adsorbing species will vary with coverage, as already noted by Reimhult et al. The hydration model provides a simple rationale to understand this phenomenon. At low coverage, the QCM response will strongly overestimate the mass of an adsorbing particle, due to the water that is present in its solvent coat. At high coverage, an adsorbing particle will displace the water that belongs to the hydration coat of particles that are already present on the surface. In this case, the QCM response may even underestimate the mass of an adsorbing particle, since only little more than the difference in density between solute and solvent is sensed. The quantitative dependence of sensitivity, defined as $s = dm_{qcm}/dm_{optic}$, on coverage is displayed in Figure S-3 in the Supporting Information for some of the investigated adsorption scenarios. We find that the sensitivity decreases considerably with coverage, between 4- and 8-fold, depending on the adsorbent type. Given the apparent generality of our model, we expect that sensitivity variations of similar magnitude will occur for many other proteins interacting with a flat surface. This phenomenon will affect the determination of kinetic constants as measured by QCM, and earlier kinetic studies (see ref 50 and many others) may need to be carefully reassessed. In this respect, the hydration model can serve as a valuable guideline.

Effects of Surface Roughness. The presented model explicitly considers the effect of surface corrugations, induced by the adsorption of solute particles, on the QCM resonance frequency shift. Inertial contributions due to coupled liquid are considered, and viscous energy dissipation caused by nonlaminar liquid motion is neglected. In our experiments, the rms-heights of the roughness varied between a few and a few tens of nanometers, while the lateral correlation length, i.e., the average spacing between adsorbent particles, decreased from ~100 nm to a few nanometers throughout the adsorption process. The successful application of the model to the experimental data suggests that inertial contributions dominate the frequency shift for this type of roughness. Similar approaches may prove useful for predicting the frequency response for applications were surfaces of similar roughness are employed.

We note that the sensor surface itself does also exhibit a slight roughness. The surface is typically made up of grains with lateral dimensions of 30−70 nm and heights of 3−5 nm, resulting in a root-mean-square roughness of around 1 nm.[46] In a simplistic approach, along the lines of our phenomenological model and considering the typical size of the employed adsorbates and their hydration coat, one may argue that particles that are adsorbed on top of a grain will have a hydration above average while those sitting in crevices have a lowered hydration. These effects will thus average out, at least partly. Given the support's rather shallow roughness and this averaging effect, we expect the effect of the sensor roughness on the QCM-D responses reported here to be rather small.

It will also be interesting to explore whether the model can be applied for larger length scales. Future theoretical efforts that rigorously treat the hydrodynamics of the shear oscillation of the QCM-D (cf. recent developments by Johannsmann et al.[55]) appear necessary and desirable to establish a physical basis for our phenomenological model and to compare our model with existing theoretical treatments (cf. refs 8 and 9 and references therein) that are more general yet less straightforward to correlate with the type of experimental data presented here.

CONCLUSIONS AND PERSPECTIVES

By employing a technical setup that combines reflectometry and QCM-D on the same support, we could quantify the variation in hydration, as sensed by QCM, as a function of coverage for several different monolayer formation scenarios. The hydration curves could be reproduced quantitatively using a model that ascribes a hydration coat, here chosen to be shaped as a truncated pyramid, to each adsorbed particle and that accounts for the random distribution of adsorbents on the surface.

The model is phenomenological. It will be interesting to see whether future simulation efforts that rigorously treat the hydrodynamics of the shear oscillation of the QCM-D sensor can provide a firm physical basis for this model. Despite its phenomenological nature, the approach provides quantitative insight into the contribution of coupled water to the QCM frequency shift. Our data suggests that, for adsorbents of a few to a few tens of nanometers in size, the hydration can be reasonably well estimated from the adsorbent's height and lateral dimensions. The aspect ratio Z, but not the adsorbent size, is determinant for the external hydration. From fits to the experimental data, we found that the minimum lateral extension of the coat is similar to the height of the adsorbent.

(48) Richter, R. P.; Maury, N.; Brisson, A. *Langmuir* **2005**, *21*, 299–304.
(49) Frey, W.; Brink, J.; Schief, W. R., Jr.; Chiu, W.; Vogel, V. *Biophys. J.* **1998**, *74*, 2674–2679.
(50) Kastl, K.; Ross, M.; Gerke, V.; Steinem, C. *Biochemistry* **2002**, *41*, 10087–10094.
(51) Tsai, J.; Taylor, R.; Chothia, C.; Gerstein, M. *J. Mol. Biol.* **1999**, *290*, 253–266.
(52) Greenwood, A. I.; Tristram-Nagle, S.; Nagle, J. F. *Chem. Phys. Lipids* **2006**, *143*, 1–10.
(53) Hendrickson, W. A.; Pahler, A.; Smith, J. L.; Satow, Y.; Merritt, E. A.; Phizackerley, R. P. *Proc. Natl. Acad. Sci. U.S.A.* **1989**, *86*, 2190–2194.
(54) Rosano, C.; Arosio, P.; Bolognesi, M. *Biomol. Eng.* **1999**, *16*, 5–12.
(55) Johannsmann, D.; Reviakine, I.; Rojas, E.; Gallego, M. *Anal. Chem.*, in press.

Our models do also suggest that the distribution of the adsorbents across the surface can influence the hydration curves appreciably, in particular at low and medium coverage. Refined models that account for particular morphological features of the interface, such as adsorbent clustering, coverage-dependent conformational states of adsorbents, or the presence of two or more adsorbing species, can provide predictions than can be directly compared with experimental hydration data. It is hoped that such approaches allow for an improved interpretation of the QCM-D response or the data obtained from combining a mass-sensitive optical technique and QCM-D. They should thus be valuable for the study of adsorption processes or conformational changes on surfaces, in particular for biosensing applications.

ACKNOWLEDGMENT

Support by Joachim Spatz (University of Heidelberg and Max Planck Institute for Metals Research, Stuttgart) is acknowledged. David J. Evans and George P. Lomonossoff are thanked for Ph.D. supervision to N.F.S. EU Grant MEST-CT-2004-504273 and the BBSRC (U.K.) are acknowledged for funding N.F.S. We thank Ixaskun Carton Telleria, Ilya Reviakine, and Patricia Wolny for critical reading and comments on the manuscript.

SUPPORTING INFORMATION AVAILABLE

Generalization and derivation of the analytical solutions for hydration model 2; sensitivities as a function of coverage for selected adsorption scenarios; in situ AFM image of a CPMV monolayer on gold; and snapshots of the arrangement of adsorbents according to the RSA model. This material is available free of charge via the Internet at http://pubs.acs.org.

Received for review June 9, 2008. Accepted August 20, 2008.

AC8011686